CHEMISTRY
A European Journal

A Journal of
ChemPubSoc Europe

Accepted Article

Title: A Simple Approach to Develop Tailored Mesoporosity in Nanostructured Heteropolysalts

Authors: Juan Alcaniz-Monge

To be cited as: *Chem. Eur. J.* 10.1002/chem.201604879

Link to VoR: http://dx.doi.org/10.1002/chem.201604879

Supported by
ACES

WILEY-VCH

10.1002/chem.201604879

WILEY-VCH

A Simple Approach to Develop Tailored Mesoporosity in Nanostructured Heteropolysalts

Juan Alcañiz-Monge,*[a] Guido Trautwein,[a] Bouchra El Bakkali,[a] and Santiago Reinoso[b]

Abstract: In this work, we describe a very simple approach to develop tailored mesoporosity in any nanostructured heteropolysalt with control over both the mesoporous volume and the pore size. This approach consisting in a treatment of the solid microporous precursor with a basic agent has been tested on the ammonium salt of the Keggin-type $[PMo_{12}O_{40}]^{3-}$ heteropolyanion, and constitutes a novel procedure for the preparation of mesoporous solids with no precedents in the literature. The results obtained in this study allows for extracting two main conclusions: (i) The micro- and mesoporosity structures in the heteropolysalt nanoparticles are independent from each other; and (ii) The development of mesoporosity in the solid material must be related with a process of alkaline degradation within the core of the nanocrystals aggregating into the particles. These results afford additional valuable information to the model of porosity that is established for heteropolysalts at present.

Introduction

Porous solids constitute a class of materials with great industrial interest due to their use in sorption processes and heterogeneous catalysis.[1] The most relevant property that make these materials suitable for both applications is to display significant microporosity (pore size < 2 nm). This feature endows the materials with a high specific surface area that allows for maximizing the number of catalytic centers in the solid. In contrast, the traditional role of mesoporosity (pore size in the range 2–50 nm) has mainly been transitional to facilitate the access of reactants into the core of the particles in which the micropores are located. However, this property has also become crucial in heterogeneous catalysis during the past two decades as it has shown up the capability to provide selectivity toward those products that can only be formed within the mesopores thanks to steric effects. In this context, the discovery in 1992 of a new type of silica with ordered mesoporous structure (MCM-41)[2] marked the origin of a new field within the materials engineering, which has resulted in a multitude of patents that illustrate the economic and technological relevance achieved.[3] Hundreds of studies on the preparation of new mesoporous materials have been reported so far,[4] and they focus not only on exploring different types of precursors (SiO_2, ZrO_2, TiO_2, carbonaceous materials), but also on developing new synthetic strategies that include template-based routes, the cooperative assembly or nano-casting approaches.[5]

Currently, there is an ongoing research effort devoted to the search of more economic and environmentally benign catalysts that could for example replace expensive noble metals or hazardous acids (H_2SO_4 or HF) in industrial processes such as the oil refinement. The most promising among such type of catalysts are those that incorporate anionic metal-oxo clusters known as polyoxometalates (POMs).[6] A thorough literature is nowadays available on the preparation and catalytic applications of such species,[7] among which the large subclass of $[XM_{12}O_{40}]^{n-}$ heteropolyanions with the well-known Keggin-type structure constitute the most relevant representatives (X = heteroatom, e.g. Al^{III}, Si^{IV}, P^{V}, Co^{III}, Zn^{II}, etc.; M = addenda metal e.g. Mo^{VI}, W^{VI}). The protonated form of these species (heteropolyacids, HPAs) behave as Brønsted acids stronger than minerals, and the clusters are able to undergo reversible uptake of several electrons in fast, multistep redox processes without substantial structural changes, in such a way that they have been long regarded as suitable electronic reservoirs.

Heteropolyacids can be solubilized in a range of solvents from water to alkanes, and this versatility has resulted in their catalytic properties having being studied mostly in homogeneous phase. For their use as heterogeneous catalysts, these species have traditionally been supported on porous solids[8] or transformed into insoluble heteropolysalts via proton–cation exchange because the solubility of a given POM can be tuned to a great extent by modifying the nature of its counterions.[9] For example, alkaline heteropolysalts are soluble in aqueous media but insoluble in organic solvents, whereas (organo)ammonium salts are less soluble in comparison, but can show good solubility in polar protic solvents in turn. Increasing the organic content in the counterion can lead to insolubility in water accompanied with good solubility in common organic solvents, as illustrated by the use of the tetra-*n*-butylammonium cation when a given POM needs to be precipitated from aqueous solution or dissolved in acetonitrile or acetone. In regard to the cationic exchange, it has been shown that the replacement of protons in HPAs with bulky monovalent cations (e.g., Cs^+, NH_4^+) results in solids with the largest values of BET specific surface area among heteropolysalts (over 100 $m^2\ g^{-1}$).[10] The most remarkable textural characteristic of these solids is their high microporosity.[9a,11] In contrast, the controlled development of mesoporosity in heteropolysalts is yet to be explored as no reports on this topic can be found in the literature to our knowledge. The existence of mesoporosity associated with voids in between particles has been described for certain nanostructured heteropolysalts,[10,11] but unfortunately, its presence has been identified as circumstantial because there is no synthetic route that can ensure the formation of such voids, much less the control over the size of mesopores.

Mesoporous materials represent promising catalysts for reactions that involve substrates with large molecular size, and

[a] Prof. J. Alcañiz-Monge, Dr. G. Trautwein, Dr. B. El Bakkali
Departamento de Química Inorgánica, Facultad de Ciencias
Universidad de Alicante
P.O. Box 99, 03080 Alicante, Spain
E-mail: jalcaniz@ua.es
[b] Dr. S. Reinoso
Institute for Advanced Materials (InaMat)
Universidad Pública de Navarra
Edificio Jerónimo de Ayanz, Campus de Arrosadia, 31006
Pamplona, Spain

Supporting information for this article is given via a link at the end of the document. It includes TEM images for some of the samples discussed in this work

in which traditional catalysts (Al_2O_3, zeolites) show great limitations due to steric hindrance.[12] Due to the lack of control in the development of mesoporosity in heteropolysalts, POM clusters must be integrated in a mesoporous material for being applied as heterogeneous catalysts when the reaction is required to take place within mesopores of well-defined size.[13] The most common route for such integration consists in the wet-impregnation of the mesoporous support (MCM-41 silica, MgO, ZrO_2, TiO_2, activated carbon) with the target POM.[14] To avoid leaching of the catalytically active clusters as the reaction proceeds, the surface of the support is often derivatized with functional groups at which POMs can get anchored,[15] as exemplified by the immobilization of 12-phosphotungstic acid in a MCM-41 silica displaying amino groups at the surface.[16] Other methods for the full integration of POM clusters into mesoporous matrices include nano-casting techniques to prepare mesoporous frameworks built up from transition-metal oxide/POM building-blocks,[17] or the direct co-polymerization of MOFs and POMs via sol-gel techniques.[18]

In a previous work, some of us demonstrated that the choice of the cationic source can determine the pore textural properties of heteropolysalt powders prepared from HPAs via proton–cation exchange. More specifically, we found that the basicity of the anion in the ammonium source has a crucial role in developing mesoporosity in nanostructured $(NH_4)_3[PMo_{12}O_{40}]$ salts prepared from $H_3[PMo_{12}O_{40}]$ through titration methods.[19] In this work, we describe a very simple approach to develop tailored mesoporosity in any heteropolysalt with control over both the mesoporous volume and the pore size. This method involves treatment of a M_n[POM] heteropolysalt at a given pH value determined with a M[B] salt in which B is a basic anion, and it constitutes a new procedure for the preparation of mesoporous solids with no precedents in the literature.

Results and Discussion

Preparation and Preliminary Characterization of Samples

A few years ago, some of us showed that both the morphology and porosity of $(NH_4)_3[PMo_{12}O_{40}]$ powders prepared from the Keggin-type $H_3[PMo_{12}O_{40}]$ HPA via proton-cation exchange greatly depends on the pH value at which the precipitation reaction is carried out, which is determined by the basicity of the $[B]^-$ anion in the cationic source and its concentration in solution.[19] We were even able to develop mesoporosity in nanostructured microporous salts when they were precipitated in aqueous media with pH values above 3.0, i.e. when the cationic source contained $[B]^-$ anions with basic properties, and the largest mesoporous volumes were obtained when the heteropolysalt was prepared by precipitation with $NH_4(CH_3CO_2)$. On the basis of these observations, a controlled development of mesoporosity in microporous heteropolysalts by treating aqueous suspensions of solid samples with a basic agent to reach pH values above 3.0 appeared plausible. To confirm our hypotheses, we selected compound $(NH_4)_3[PMo_{12}O_{40}]$ (hereon referred to as **POM**) as precursor, which is known to display the largest porosity among heteropolysalts,[9a,10,11] and undergone a systematic study on the variation of its textural properties upon controlled treatment with $NH_4(CH_3CO_2)$ as the basic agent. We focused our studies on the influence of two reaction parameters: the final pH of the suspension, which is a function of the amount of basic agent used, and the reaction time.

The microporous form of the **POM** precursor was prepared as a yellow powder composed of nanoparticles with sizes in the 50–2000 nm range by following literature methods that involve acid-base titration between aqueous solutions of $H_3[PMo_{12}O_{40}]$ and the NH_4Cl cationic source, which contains a type of $[B]^-$ anion with no basic properties.[19,20] The powder was then supended in water, treated with different amounts of $NH_4(CH_3CO_2)$, recovered by filtration and dried at 120 °C. Twelve different samples were prepared by varying the homogenization times from 5 to 900 s, as well as the amount of basic agent to adjust the pH of the mixture to values in the 2.0–4.5 range (Table 1). These samples were characterized by analytical techniques (ICP-AES, CHN) and PXRD to determine whether their composition and structure was modified upon treatment. These methods revealed virtually identical chemical composition for all of the samples and negligible changes relative to that of the **POM** precursor. No traces of acetate were analytically detected.[21] The PXRD patterns remained also unaltered upon treatment with the basic agent (Figure 1). Therefore, the twelve $(NH_4)_3[PMo_{12}O_{40}]$ samples prepared in this work are analogous to the **POM** precursor in terms of the chemical composition and the crystalline structure as these characteristics were not affected by the reaction parameters subject of study (pH and homogenization time).

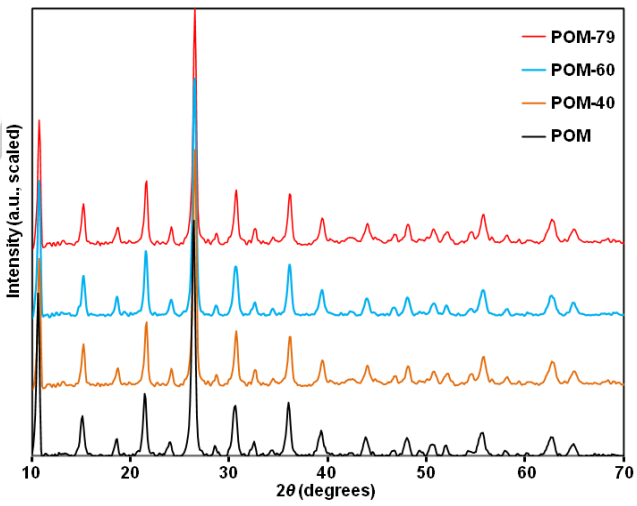

Figure 1. PXRD pattern of the original $(NH_4)_3[PMo_{12}O_{40}]$ precursor (**POM**) compared with those of the samples in which 40, 60 and 79% of the initial mass is lost upon treatment with ammonium acetate (**POM-40**, **POM-60**, and **POM-79**).

In spite of the preservation of the composition and structure, the significant variations observed in the yields obtained under different preparative conditions unequivocally indicate that the precursor is indeed affected by treatment with $NH_4(CH_3CO_2)$.

The yields obtained for the different solid samples (Table 1) reveal a loss of mass relative to the initial amount of heteropolysalt that increases with longer homogenization times and higher pH values, which is indicative of a chemical reaction taking place during the treatment. While variations between the initial amount of precursor and that of the recovered solid samples are virtually negligible for pH values below 3.0, in more basic conditions the heteropolysalt undergoes mass losses that are substantially accelerated with increases of just 0.5 units of the pH, in such a way that only a 25% of the initial amount is recovered after a treatment of just 10 s at pH 4.5. As shown in Figure 2, the loss of mass in the pH range 3.5–4.0 appears to be exponentially related with the homogenization time.

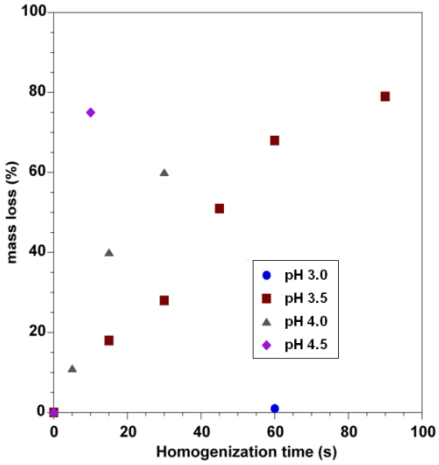

Figure 2. Time dependence of the mass loss undergone by the $(NH_4)_3[PMo_{12}O_{40}]$ precursor (**POM**) upon treatment with ammonium acetate at different pH values.

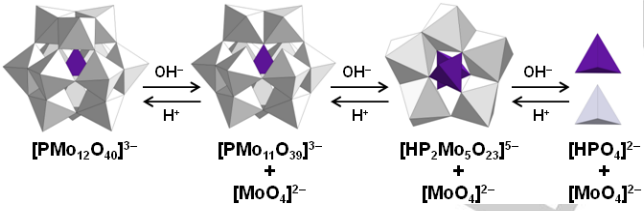

Scheme 1. Alkaline degradation of the Keggin-type $[PMo_{12}O_{40}]^{3-}$ anion into simple oxoanions as previously proposed in the literature.[22]

The observations above indicate that the type of reaction taking place during treatment with $NH_4(CH_3CO_2)$ is likely related with the solution stability of the Keggin-type $[PMo_{12}O_{40}]^{3-}$ cluster, which is highly dependent on the pH. Literature reports on the stability of Keggin-type HPAs in diluted aqueous solution (< 10^{-3} M) have shown that they are stable in highly acidic conditions but gradually degradate into other species through alkaline hydrolysis of M–O–M bonds as the pH increases.[22] Focusing on the $[PMo_{12}O_{40}]^{3-}$ anion, this plenary cluster composed of four $\{Mo_3O_{13}\}$ trimers of edge-sharing $\{MoO_6\}$ octahedra that arrange in ideal T_d symmetry around a central $\{PO_4\}$ heterogroup via corner-sharing (Scheme 2) is the predominant species in solution at pH < 2, but transforms into the lacunary derivative $[PMo_{11}O_{39}]^{7-}$ in the pH range 3–5. This derivative is formed by removal of one Mo center upon hydrolysis of four M–O–M and one M–O–P bonds, in such a way that a vacant metal position is created in the Keggin framework. At less acidic conditions, further hydrolysis leads to the conversion of the Keggin-type species into a different cluster, namely the Strandberg-type $[HP_2Mo_5O_{23}]^{5-}$, the skeleton of which consists of a ring of five $\{MoO_6\}$ octahedra capped with two $\{PO_4\}$ heterogroups. At pH > 6, the breakdown of the cluster framework is completed and $[MoO_4]^{2-}$ and $[HPO_4]^{2-}$ oxoanions coexist in solution. These studies cannot be extrapolated to our system straightforwardly, but nevertheless, it is plausible that the nanoparticles forming our heteropolysalt precursor undergo such kind of alkaline degradation, and hence, that the loss of mass upon attack of basic $(CH_3CO_2)^-$ anions originates from solubilization of the hydrolyzed products.

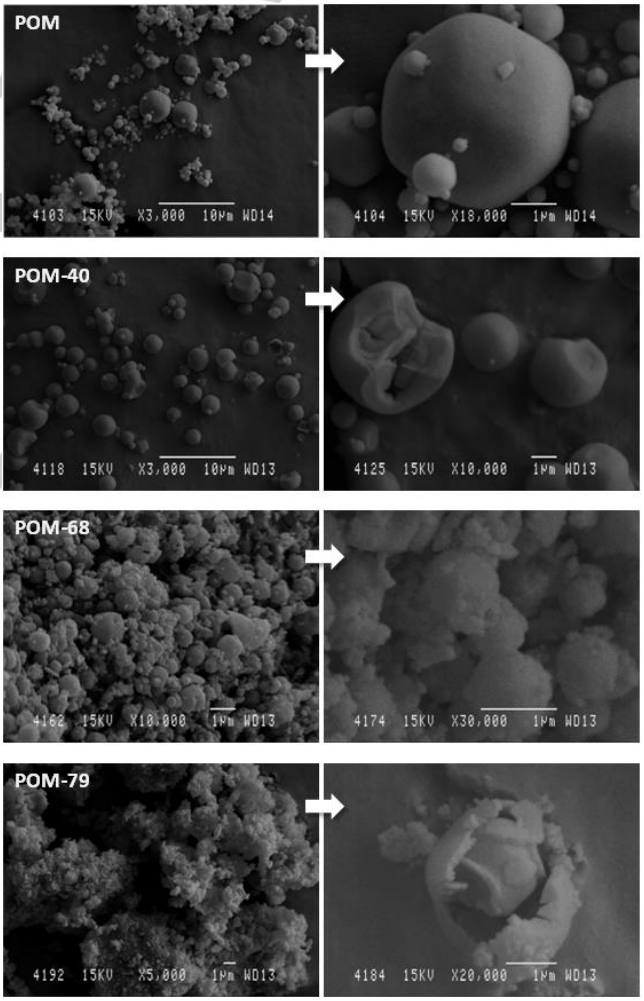

Figure 3. SEM images of the $(NH_4)_3[PMo_{12}O_{40}]$ precursor (**POM**) compared with those of the samples in which 40, 68 and 79% of the initial mass is lost upon treatment with $NH_4(CH_3CO_2)$ (**POM-40**, **POM-68**, and **POM-79**).

Morphological Analysis through SEM

The morphology of the heteropolysalt nanoparticles forming the solids prepared in this work has been investigated through SEM, and Figure 3 displays comparative images for some of the most representative samples. For the precursor, a heterogeneous distribution of nanoparticles with well-defined polyhedral geometry is observed.[10a,19] The particle sizes range from 100 to 2000 nm, but the most abundant are those with a diameter around 300 nm. Upon treatment of the **POM** suspension with $NH_4(CH_3CO_2)$, the particles undergo substantial morphological modifications in both their geometry and size, which are clearly related with the mass losses as they become more pronounced with longer homogenization times and higher pH values. In the case of the **POM-40** sample, most of the particles retain their characteristic morphology despite a mass loss of 40%, but burst species can already be observed. The amount of broken particles, as well as the extent of the fractures, increases with the mass losses becoming larger and for the **POM-68** sample the material is mainly composed of small broken pieces, although a noticeable number of particles still retain their initial size and morphology. The largest mass loss is achieved for the **POM-79** sample, which consists in a highly dispersed material composed of flakes that derive from the burst particles.

Analysis of the Pore Texture through Gas Sorption

The porous texture of the **POM** precursor and those of the samples obtained upon treatment with $NH_4(CH_3CO_2)$ were investigated through gas sorption measurements of N_2 at –196 ºC and CO_2 at 0 ºC. Figure 4 shows the isotherms of N_2 adsorption, the following features of which are worth noting: (i) The magnitude of the adsorption at a relative pressure P/P_o < 0.3, which associates with the specific microporous volume; (ii) The shape of the isotherm elbow, which is related with the distribution of the micropore sizes; (iii) The magnitude of the adsorption at a relative pressure P/P_o > 0.3; and (iv) The presence of hysteresis in the adsorption-desorption cycles, which is indicative of mesopores existing in the material.

The **POM** precursor shows adsorptive properties only at low relative pressures (P/P_o < 0.2) and the curve displays the characteristic features of a Type I isotherm according to the IUPAC classification.[23] This confirms the essential microporous nature of the heteropolysalt precursor as previously noted in the literature.[19,20] In the case of the samples prepared in this work, the elbows of the isotherms (P/P_o < 0.3) are nearly identical to that displayed by the **POM** precursor for those solids in which mass losses up to 40% have taken place. This fact is indicative of the microporosity not being affected by the basic treatment for these particular samples. In contrast, a gradual decrease of the sorption capacity in this P/P_o range is observed for those samples corresponding to mass losses larger than 40%. This decrease in the sorption capacity at low relative pressures becomes more pronounced as the mass loss increases, and it is accompanied by a concomitant gradual increase of the N_2 adsorption in the P/P_o > 0.3 region. This behavior reveals a clear change in the porous texture that associates with the existence of mesoporosity in these largely hydrolyzed samples. The appearance of hysteresis cycles in the adsorption-desorption isotherms further confirms the development of internal mesoporosity within the samples upon basic treatment.[23,24,25] The volume of developed mesoporosity is correlated with the mass loss undergone by the solid samples during their preparation and reaches its maximum value for the **POM-60** sample. Focusing on the shape of the isotherms in the P/P_o > 0.3 region, it can also be noticed that the hysteresis cycles broaden as the mass loss increases, in such a way that they progressively cover higher relative pressures. These observations suggest a controlled development of the size of the mesoporosity, and to achieve further insight on this behavior, the N_2 adsorption data were analyzed through the BJH method to calculate the distribution of the mesopore sizes.[26]

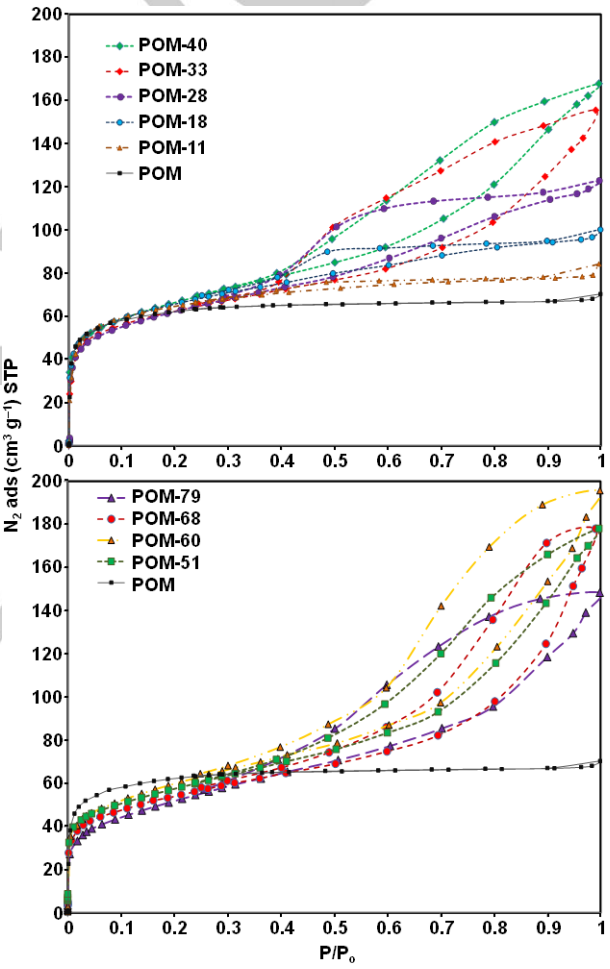

Figure 4. Isotherm of N_2 adsorption at –196 ºC for the $(NH_4)_3[PMo_{12}O_{40}]$ precursor (**POM**) compared with those for nine amongst the samples prepared in this work in which the mass losses upon treatment with $NH_4(CH_3CO_2)$ range from 11 to 79% (**POM-11** to **POM-79**).

As shown in Figure 5, all of the samples prepared in this work display well-defined bands for the pore size distribution (PSD) that appear around delimited pore size values. This indicates a development of mesopores with preferential sizes that relates with the amount of mass lost during their preparation.

Indeed, the PSD bands become broader and their maxima shift to higher values of the pore size as the mass loss increases. Therefore, the latter represents a suitable experimental parameter to estimate and to control the size of the mesoporosity that can be developed in solid heteropolysalts treated with a basic agent. The analysis of the displacement of the maxima of the PSD bands toward larger pore sizes follows a well-defined trend from 3 to 6, 9, 12 and 15 nm as the mass losses increase. This trend suggests that the degradation of the nanoparticles under our preparative conditions is not as random as the SEM images (Figure 3) could indicate at a first glance, but proceeds through the release of structural units with preferential sizes. The fact that intact nanoparticles coexist with small broken pieces for samples that have undergone mass losses above 40% can then be explained on the basis of the vigorous stirring applied during their preparation: as a result of the release of well-defined structural units upon alkaline degradation, the nanoparticles become progressively more fragile and can therefore be fractured mechanically with more ease to lead to larger amounts of broken pieces or even flakes.

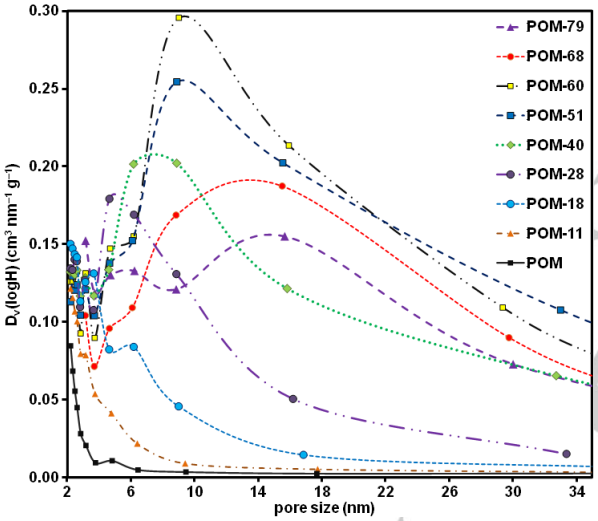

Figure 5. Distribution of the mesopore sizes obtained by applying the BJH method to the isotherms of N_2 adsorption in Figure 4.

To analyze further the development of mesoporosity in our samples, the narrow microporous volume ($V(CO_2)$) has been calculated from the CO_2 sorption data,[27] together with the total microporous ($V(N_2)$) and mesoporous (V(meso)) volumes from the N_2 sorption isotherms. As shown in Figure 6, the microporous narrow and total volumes are slightly above 0.08 and 0.10 cm^3 g^{-1} for the **POM** precursor, respectively, and they do not undergo significant variations for those samples corresponding to mass losses up to as much as 40% (ca. ±0.005 cm^3 g^{-1} at the most). For larger mass losses, both magnitudes decrease moderately in a nearly parallel fashion to reach minimum values slightly above 0.04 cm^3 g^{-1} for the narrow $V(CO_2)$ (variation of ca. 0.04 cm^3 g^{-1} with respect to the initial value that accounts for a −45%) and ca. 0.09 cm^3 g^{-1} for the total $V(N_2)$ (variation of slightly less than 0.02 cm^3 g^{-1} that accounts for a −19%). Considering that the total $V(N_2)$ encompasses the narrow $V(CO_2)$, this behavior reveals that the decrease in the microporous volume is almost exclusively due to the narrow microporosity (< 0.7 nm), while micropores with sizes in the 0.7–2 nm range remain virtually unmodified even in samples corresponding to mass losses as large as ca. the 80% of the initial amount of precursor. In contrast, the mesoporosity evolves following a completely different trend. The mesoporous volume of the **POM** precursor is almost null but increases substantially as the mass loss becomes larger. The maximum V(meso) value of ca. 0.20 cm^3 g^{-1} is reached when 60% of the initial mass of precursor is lost upon basic treatment (variation of +193% with respect to the total initial volume of mesopores). For larger mass losses, V(meso) undergoes significant decrease to reach a minimum value around 0.14 cm^3 g^{-1} for the **POM-79** sample (variation of ca. 0.06 cm^3 g^{-1} that accounts for a −58%). Therefore, it is clear that the mesoporous volume developed in our samples cannot be correlated with the lost of microporosity undergone by the heteropolysalt upon basic treatment.

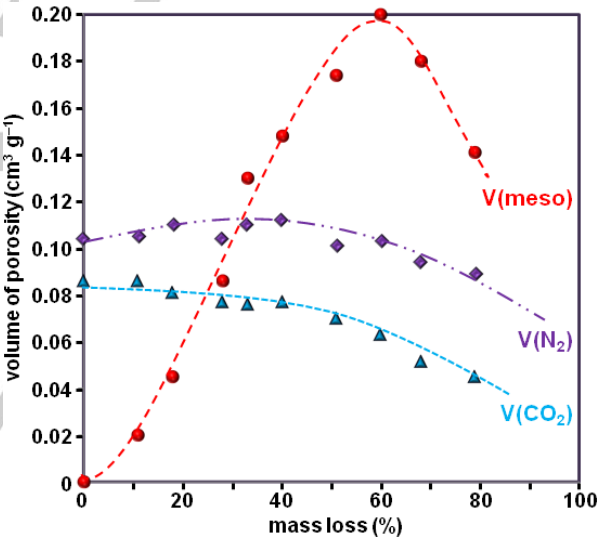

Figure 6. Evolution of the microporous ($V(CO_2)$, narrow; $V(N_2)$, total) and mesoporous (V(meso)) volumes with the mass loss undergone by the **POM** precursor upon basic treatment.

Nanoparticle Analysis through TEM

To confirm the results above, the solids were analyzed through TEM and Figure 7 displays comparative images for some of the most representative samples. The TEM images evidence that (i) the mass losses proceed gradually and homogeneously within the nanoparticles; and (ii) they involve the constituent nanocrystals undergoing progressive degradation until complete dissolution. The TEM images of the **POM** sample are in agreement with the SEM results and with the characterization of analogous samples in the literature,[19,28] as they show that the precursor is composed of nanoparticles with dodecahedral shape and a heterogeneous size distribution in the 50 to 2000

nm range. The nanoparticles are fully opaque, which indicates a dense and compact packing that cannot be crossed by the electron beam. A zoom into the particles reveals corrugated surfaces with a random distribution of darker and brighter areas with pseudo-spheric geometry and sizes of ca. 10 nm. These features are fully consistent with the model proposed by Mizuno and Misono,[6a] in which nanostructured heteropolysalt particles consist in aggregates of nanocrystals with sizes in the 5–20 nm range that would lead to the dark areas in the TEM images.[28]

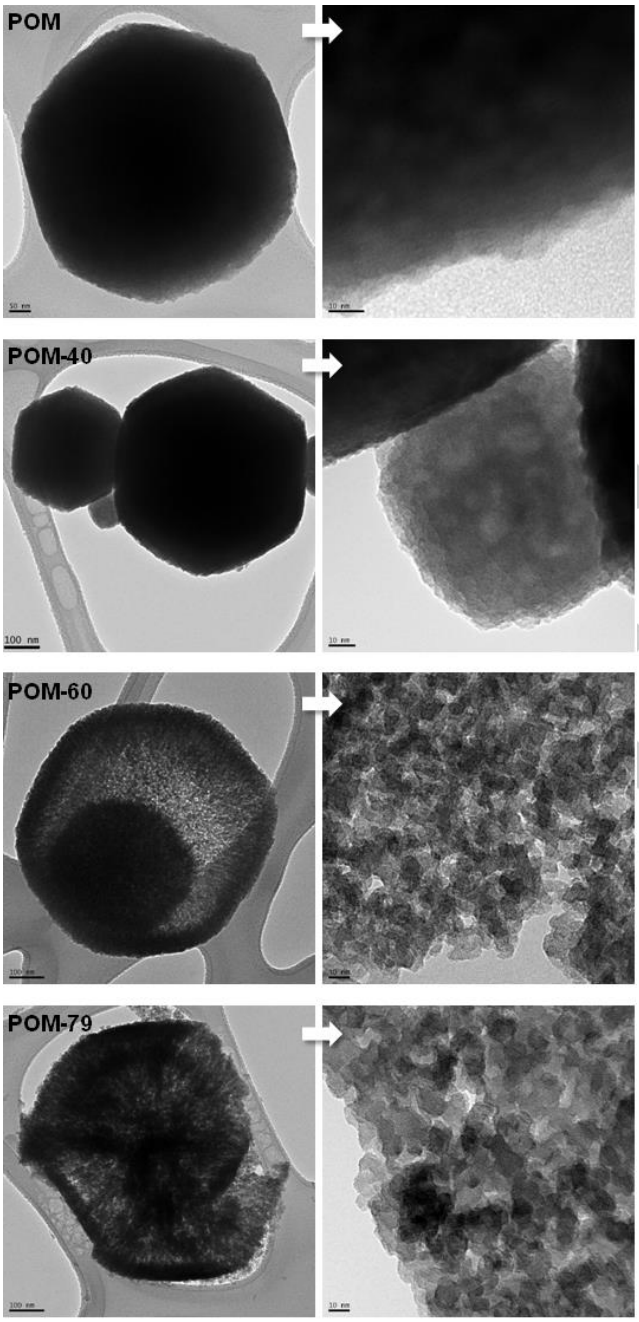

Figure 7. TEM images of the $(NH_4)_3[PMo_{12}O_{40}]$ precursor (**POM**) compared with those of the samples in which 40, 60 and 79% of the initial mass is lost upon treatment with $NH_4(CH_3CO_2)$ (**POM-40**, **POM-60**, and **POM-79**). Resolution: 100 nm in the left column (50 nm for the **POM** precursor) and 10 nm in the right column.

In the case of the **POM-40** sample, the nanoparticles closely resemble those observed for the **POM** precursor in spite of the material having undergone a mass loss of 40%. The dodecahedral morphology and the lack of transparency is fully preserved. Nevertheless, some differences can be noticed upon close inspection of the corrugated surfaces. The nanoparticles now display a significantly less compact packing as indicated by a higher number of bright areas that are distributed over the entire particle surface. The additional loss of a 20% of the mass (**POM-60** sample) induces substantial modifications that can be identified without the need of any zoom in (Figure S1 in the Supporting Information). The morphology is still reasonably maintained at this stage but the existence of internal porosity within the nanostructured material can be clearly noticed on the basis of all nanoparticles showing inner bright areas, and a much brighter shell as a result of a larger extent of alkaline degradation taking place at the outermost area due to the surface being in direct contact with the reaction medium. The degradation proceeds toward the particle inside and delves into the innermost part following a preferential pattern, as a radial arrangement of strings made of chained bright areas that converge toward a dark central core is observed.

It is worth reminding that the mass losses determined in our study are average values obtained for materials composed of particles with heterogeneous size distributions, and hence, that the smallest nanoparticles in the material will undergo more pronounced degradation than the largest ones. The image included in Figure 7 corresponds to a single particle among the smallest found for the **POM-60** sample and exemplifies how they are affected by larger extents of alkaline degradation. In this case, the radial arrangement of bright strings converging in a central dark core is replaced with a homogeneous distribution of bright areas within the entire particle that is characteristic of a light, fluffy packing with remarkable porosity. All of the bright areas are similar in size with dimensions slightly below 10 nm and this observation is in full agreement with the results obtained from the distribution of the mesopore sizes (Figure 5), which showed the maximum of the PSD band around 9 nm. Thus, each of these void spaces could be associated with the full degradation of a constituent nanocrystal. This process is likely to develop in the bosom of each of such well-defined structural units according to the lighter color observed for the remaining nanocrystals in the particle. For mass losses larger than 60% (**POM-79** sample), most of the particles burst into pieces to lead to a solid material composed mainly of flakes as shown by SEM (Figure 3). According to the TEM images (Figure S2 in the Supporting Information), these flakes are extremely thin and display very high porosity, in such a way that the structure of the support used for the image acquisition can be clearly noticed through the heteropolysalt sheets. Images for one of the scarce nanoparticles that still retained certain integrity in the **POM-79** sample are included in Figure 7. The shape of these particles is partially lost and they appear as partially

broken. Close inspection of these fragmented species reveals bright areas that are lighter in color and larger in extension than those of **POM-60**, which is consistent with the maximum of the PSD band being centered at 15 nm according to the results from the distribution of the mesopore sizes (Figure 5).

Discussion of the Trends Observed in the Evolution of the Porosity

The analysis of our samples through a combination of the results obtained from the porous textural characterization, variation in the volumes of porosity and pore size distributions, and TEM images allows for extracting two main conclusions: (i) The micro- and mesoporosity structures present in the heteropolysalt nanoparticles that form our samples are independent from each other; and (ii) The existence of mesoporosity in the materials must be related with the alkaline degradation that the constituent nanocrystals of the particles undergo upon interaction with the basic agent during the preparation procedure.

In regard to conclusion (i), we think our results afford additional valuable information to the model of porosity that is established for heteropolysalts at present. The seminal studies of microporosity in POM salts indicated that this property was restricted to salts of Keggin-type clusters with bulky cations (K^+, Cs^+, Rb^+, NH_4^+).[29] As a result of this specificity, the textural studies developed from the mid 80s to the late 90s on such materials were mainly focused on demonstrating whether microporosity was implicit as postulated by Moffat and coworkers,[10a,c] or explicit, the main contributions to this hypothesis corresponding to Misono and coworkers.[6a,11] The former implicit model considers the porosity present in hetropolysalts as originating from the crystallographic structure and being a direct consequence of the existence of accessible voids in the crystal packing in close analogy with certain open-framework crystalline materials such as zeolites or clays. The latter explicit model considers the porosity as external to the crystal packing, and hence, originating from a hierarchical structure organized in the following three levels: primary, that corresponds to the framework of the Keggin clusters; secondary, that is equivalent to the crystallographic structure and corresponds to the formation of ionic nanocrystals of Keggin-type anions and bulky cations packed in a body-centered cubic lattice; and tertiary, that corresponds to the self-assembly of nanocrystals with sizes in the 5–20 nm range[28] that aggregate epitaxially following a regular pattern to grow nanoparticles with well-defined polyhedral geometry similar to those shown in Figure 3. According to Misono's explicit model, the porosity originates from the accessible voids left amongst nanocrystals upon epitaxial aggregation. This model is the most accepted at present, but both implicit and explicit interpretations are supported by solid experimental evidences. However, neither model is suitable for affording a reasonable explanation to the fact that highly porous heteropolysalts can only be obtained with monovalent cations of radii in the 0.27–0.34 nm range.[10a]

In this work, the precursor is an essentially microporous heteropolysalt, the porosity of which originates from accessible voids amongst nanocrystals aggregating into dodecahedral particles according to Misono's model. We have established a direct relationship between the development of mesoporosity in such nanoparticles and the loss of mass undergone by their constituent nanocrystals upon alkaline degradation. From our viewpoint, the only suitable explanation for the independent trends observed in the variation of the micro- and mesoporosity with the loss of mass is to consider that the latter takes place preferentially in the innermost part of the nanocrystals as the TEM images suggest. Thus, implicit mesoporosity developes within the nanocrystal cores as the alkaline degradation acts up to mass losses around 40%, while the explicit microporosity remains nearly unaltered due to the outermost shell of the nanocrystals, and hence the voids amongst them in the epitaxial aggregates, being essentially preserved during the process. The following additional results support this interpretation. The He density of the crystallographic packing in the nanocrystals is 3.6 g cm^{-3} and this value is maintained unaltered in our samples. Therefore, 0.4 g of the precursor (equivalent to a 40% of the initial mass) would occupy a volume of 0.11 cm^3 g^{-1}. When this mass is lost due to degradation, the volume left void upon normalization would be 0.18 cm^3 g^{-1} considering that the nanoparticle structure is preserved as indicated by SEM and TEM analyses. This value is comparable to the experimental mesoporous volume of the **POM-40** sample in Figure 6 (0.15 cm^3 g^{-1}) and confirms that degradation is mainly localized within the nanocrystals. For mass losses larger than 40%, the mesoporous volume continues developing while the microporous volume becomes gradually smaller. This behavior is consistent with a progressive disruption of the structure in which the nanocrystals aggregate as shown by SEM and TEM images. In the case of further mass loss, two opposite effects start competing: (1) internal degradation of large nanocrystals, which allows mesoporosity to develop further; and (2) full degradation of small nanocrystals, which weakens the structure of the nanoparticles, triggers their breakdown and collapse, and consequently, induces a decrease of the associated micro- and mesoporosity. These two effects explain the maximum in the development of mesoporosity observed for the **POM-60** sample (Figure 6), as well as its decline for mass losses beyond.

Conclusions

A new preparative procedure for the controlled development of mesoporosity in microporous heteropolysalts is established. This procedure consists in treating aqueous suspensions of the nanostructured heteropolysalt precursor with a basic agent, which greatly affects the mesoporous volume and the pore size. The volume of developed mesoporosity was found to be strongly correlated with the mass lost by the precursor upon basic treatment. The TEM images evidence that the mass losses proceed gradually and homogeneously within the nanoparticles. Both facts indicate that the existence of mesoporosity in the heteropolysalts must be related with a process of alkaline degradation taking place in the core of the nanocrystals that aggregate into the particles. The results obtained in this work remark that the micro- and mesoporosity structures present in the nanoparticles are independent from each other.

Experimental Section

Materials. All reagents were purchased from commercial sources and used without purification. The $(NH_4)_3[PMo_{12}O_{40}]$ precursor (**POM**) was prepared in microporous form according to a method that has been described previously in the literature.[19,20] This method involves the acid-base titration of the $H_3[PMo_{12}O_{40}]$ heteropolyacid with NH_4Cl in aqueous medium and affords a yellow powder made of nanoparticles with sizes in the 50–2000 nm range.

Preparation of Samples. The **POM** precursor (1 g, 0.53 mmol) was suspended in water (25 mL), acidified to pH 1.5 with concentrated HCl (1.4 mL), and heated to 60 ºC. The pH of this suspension was adjusted to a value in the 2.0–4.5 range by rapid addition under vigorous stirring (1200 rpm) of an aqueous 0.2 M solution of $NH_4(CH_3CO_2)$. The mixture was homogenized and stirred for a period of time ranging from 10 to 900 s, and then, the resulting yellow solid was filtered off in vacuo, washed with acidified water (pH 2.0), and dried overnight in an oven at 120 ºC. Twelve different $(NH_4)_3[PMo_{12}O_{40}]$ samples have been obtained by varying the pH value to which the suspension is adjusted and the period of time along which the mixture is homogenized. The samples differ in the percentage of mass that the **POM** precursor losses upon treatment with ammonium acetate (ie. **POM-60** is the sample in which the precursor undergoes a 60% loss of the initial mass during the preparative procedure described above). Table 1 summarizes the pH and reaction time conditions that were applied to prepare the title twelve samples, as well as the mass losses calculated for each sample.

Table 1. pH values and homogenization times applied in the preparation of the $(NH_4)_3[PMo_{12}O_{40}]$ samples studied in this work, together with mass Losses undergone by the precursor during treatment with $NH_4(CH_3CO_2)$.

sample	pH	reaction time (s)	mass loss (%)
POM	2.0	900	0
POM-1	3.0	60	1
POM-3		300	3
POM-18	3.5	15	18
POM-28		30	28
POM-51		45	51
POM-68		60	68
POM-79		90	79
POM-11	4.0	5	11
POM-40		15	40
POM-60		30	60
POM-75	4.5	10	75

Characterization Techniques. The Mo and P content was determined by Inductive Coupling Plasma-Atomic Emission Spectrometry (ICP-AES) using a Perkin Elmer 7300 DV spectrometer. The CHN elemental analyses were carried out in a Carlo Erba EA 1110 CHNS-O equipment. Powder X-ray diffraction (PXRD) patterns were collected in a Seifiert JSO Debye-Flex 2002 diffractometer equipped with Cu Kα radiation. Scanning Electron Microscopy (SEM) and Transmission Electron Microscopy (TEM) images were recorded on Hitachi S-3000N and JEOL JEM-2010 instruments, respectively.

The solid framework densities were determined on the basis of He displacement in an AccuPyc 1330 Micrometrics equipment. The solid samples (0.5 g) were previously outgassed in vacuo at 150 ºC for 12 h. The porous textures were characterized through gas adsorption measurements (N_2 at –196 ºC and CO_2 at 0 ºC) using the volumetric equipments Autosorb 6-B and Autosorb-6, respectively.[27] The solid samples (0.2 g) were previously outgassed in vacuo at 150 ºC for 4 h. The specific surface areas were determined by applying the Brunauer-Emmet-Teller (BET) equation.[30] The Dubinin-Radushkevich (DR) equation was used to calculate the microporous volume,[31] whereas the mesopororous volume was determined from the De Boer method.[24] The distribution of the mesopore sizes was determined from the isotherms of N_2 adsorption by applying Barrett-Joyner-Halenda (BJH) method.[26]

Acknowledgements

This work was financially supported by Generalitat Valenciana (grant PROMETEO2/2014/010) and Ministerio de Economia y Competitividad (grant CTQ2015-64801-R) through FEDER funds.

Keywords: Polyoxometalates • Mesoporous materials • Microporous materials • Adsorption • Electron microscopy

[1] a) *Handbook of Porous Solids* (Eds.: F. Schüth, K. W. Sing, J. Weitkamp), Wiley-VCH, Weinheim, Germany, **2002**; b) *Handbook of Heterogeneous Catalysis,* 2nd Edition (Eds.: G. Ertl, H. Knözinger, F. Schüth, J. Weitkamp), Wiley-VCH, Weinheim, Germany, **2008**.

[2] J. S. Beck, C. T. W. Chu, I. D. Johnson, C. T. Kresge, M. E. Leonowicz, W. J. Roth, J. C. Vartuli, WO Patent 91/11390, **1991**.

[3] See for example: a) S. Beck, C. T. W. Chu, I. D. Johnson, C. T. Kresge, M. E. Leonowicz, W. J. Roth, J. C. Vartuli, U.S. Patent 5,108,725, **1992**; b) J. S. Beck, K. D. Smith, J. C. Vartuli, U.S. Patent 5,334,368, **1994**; c) P. J. Nat, E. T. C. Wogt, WO Patent 94/26847, **1994**; d) J. S. Beck, C. T Kresge, S. B. McCullen, W. J. Roth, J. C. Vartuli, U.S. Patent 5,370,785 **1994**; e) T. F. Degnan, Jr., K. M. Keville, M. E. Landis, D. O. Marler, D. N. Mazzone, U.S. Patent 5,290,744, **1994**; f) U. Müller, B. Reck, J. Roser, U.S. Patent 5,951,962, **1997**; g) S. Kaliaguine, T. Do, U.S. Patent 6,669,924, **2003**; h) Y. Tao, H. Kanoh, K. Kaneko, U.S. Patent 6,998,104, **2006**; i) J. J. Watkins, R. Pai, U.S. Patent 7,419,772, **2008**.

[4] For some relevant books and reviews see: a) A. Corma, *Chem. Rev*. **1997**, *97*, 2373–2420; b) R. Anwander, *Chem. Mater*. **2001**, *13*, 4419–4438; c) X. He, D. Antonelli, *Angew. Chem. Int. Ed*. **2002**, *41*, 214–229; d) A. P. Wight, M. E. Davis, *Chem. Rev*. **2002**, *102*, 3589–3614; e) D. E De Vos, M. Dams, B. F. Sels, P. A. Jacobs, *Chem. Rev*. **2002**, *102*, 3615–3640; f) G.-J. de A. A. Soler-Illia, C. Sanchez, B. Leveau, J. Patarin, *Chem. Rev*. **2002**, *102*, 4093–4138; g) A. Taguchi, F. Schüth, *Microporous Mesoporous Mater*. **2005**, *77*, 1–45; h) *Recent Progress in Mesostructured Materials* (Eds.: D. Zhao, S. Qiu, Y. Tang, C. Yu), Studies in Surface Science and Catalysis 165, Elsevier, Amsterdam, The Netherlands, **2007**; i) *Ordered Porous Solids. Recent Advances and Prospects* (Eds.: V. Valtchev, S. Mintova, M. Tsapatsis), Elsevier, Amsterdam, The Netherlands, **2009**.

[5] See for example: a) V. R. Choudhary, S. K. Jana, B. P. Kiran, *J. Catal*. **2000**, *192*, 257–261; b) R. Raja, T. Khimyak, J. M. Thomas, S. Hermans, B. F. G. Johnson, *Angew. Chem. Int. Ed*. **2001**, *40*, 4638–4642; c) X. Gao, I. E. Wachs, M. S. Wong, J. Y. Ying, *J. Catal*. **2001**,

203, 18–24; d) K. Zhu, B. Yue, W. Zhou, H. He, *Chem. Commun*. **2003**, 98–99; e) B. Tian, X. Liu, H. Yang, S. Xie, C. Yu, B. Tu, D. Zhao, *Adv. Mater.* **2003**, *15*, 1370–1374; f) K. Lee, Y.-H. Kim, S. B. Han, H. Kang, S. Park, W. S. Seo, J. T. Park, B. Kim, S. Chang, *J. Am. Chem. Soc*. **2003**, *125*, 6844–6845; g) H. Yang, Q. Shi, B. Tian, Q. Lu, F. Gao, S. Xie, J. Fan, C. Yu, B. Tu, D. Zhao, *J. Am. Chem. Soc*. **2003**, *125*, 4724–4725; h) B. Tian, X. Liu, L. A. Solovyov, Z. Liu, H. Yang, Z. Zhang, S. Xie, F. Zhang, B. Tu, C. Yu, O. Terasaki, D. Zhao, *J. Am. Chem. Soc*. **2004**, *126*, 865–875.

[6] a) N. Mizuno, M. Misono, *Chem. Rev*. **1998**, *98*, 199–217; b) J. B. Moffat, *Metal-Oxygen Clusters: The Surface and Catalytic Properties of Heteropoly Oxometalates*, Springer, New York, USA, **2001**; c) I. V. Kozhevnikov, *Catalysts for Fine Chemical Synthesis, Volume 2, Catalysis by Polyoxometalates*, John Wiley & Sons, Chichester, UK, **2002**.

[7] a) M. T. Pope, *Heteropoly and Isopoly Oxometalates,* Springer-Verlag, Berlin, Germany, **1983**; b) C. L Hill (Guest Ed.), *Chem. Rev*. **1998**, vol. 98, issue 1 (thematic issue), pp. 1–387; c) *Polyoxometalates: from Platonic Solids to Anti-Retroviral Activity* (Eds.: M. T. Pope, A. Müller), Kluwer, Dordrecht, The Netherlands, **1994**; d) *Polyoxometalate Chemistry for Nano-Composite Design* (Eds.: T. Yamase, M. T. Pope), Kluwer, Dordrecht, The Netherlands, **2002**; e) *Polyoxometalate Molecular Science* (Eds.: J. J. Borrás-Almenar, E. Coronado, A. Müller, M. T. Pope), Kluwer, Dordrecht, The Netherlands, **2003**; f) L. Cronin, A. Müller (Guest Eds.), *Chem. Soc. Rev*. **2012**, *41*, issue 22 (thematic issue), pp. 7325–7648; g) *Polyoxometalate Chemistry: Some Recent Trends* (Ed.: F. Sécheresse), World Scientific, Singapore, **2013**.

[8] See for example: a) J. Alcañiz-Monge, G. Trautwein, J. P. Marco-Lozar, *Appl. Catal. A* **2013**, *468*, 432–441; b) L. R. Pizzio, P. G. Vázquez, C. V. Cáceres, M. N. Blanco, *Appl. Catal. A* **2003**, *256*, 125–139.

[9] See for example: a) J. Alcañiz-Monge, G. Trautwein, A. García-García, *J. Mol. Catal. A Chem*. **2014**, *394*, 211–216; b) G. Trautwein, B. El Bakkali, J. Alcañiz-Monge, B. Artetxe, S. Reinoso, J. M. Gutiérrez-Zorrilla, *J. Catal*. **2015**, *331*, 110–117.

[10] a) J. B. McMonagle, J. B. Moffat, *J. Colloid Interface Sci*. **1984**, *101*, 479–488; b) M. Yoshimune, Y. Yoshinaga, T. Okuhara, *Microporous Mesoporous Mater*. **2002**, *51*, 165–174; c) J. B. Moffat, *J. Mol. Catal*. **1989**, *52*, 169–191; d) D. Lapham, J. B. Moffat, *Langmuir* **1991**, *7*, 2273–2278.

[11] T. Okuhara, N. Mizuno, M. Misono, *Adv. Catal*. **1996**, *41*, 113–252.

[12] a) C. T. Kresge, M. E. Leonowicz, W. J. Roth, J. C. Vartuli, J. S. Beck, *Nature* **1992**, *359*, 710–712; b) N. Shetti, J. Kim, R. Srivastava, M. Choi, R. Ryoo, *J. Catal*. **2008**, *254*, 296–303.

[13] G. S. Armatas, *New and Future Developments in Catalysis. Hybrid Materials, Composites, and Organocatalysts* (Ed.: S. L. Suib), Elsevier, Amsterdam, The Netherlands, **2013**, ch. 13, pp. 311–342.

[14] a) W. E. Farneth, R. J. Gorte, *Chem. Rev*. **1995**, *95*, 615–635; b) B. B. Bardin, S. V. Bordawekar, M. Neurock, R. J. Davis, *J. Phys. Chem. B* **1998**, *102*, 10817–10825; c) R. M. Richards, U. Kortz, L. Bi, K. Zhu, U.S. Patent 7,417,008, **2008**.

[15] J. Hu, K. Li, W. Li, F. Ma, Y. Guo, *Appl. Catal. A* **2009**, *364*, 211–220.

[16] R. Gao, Q. Zhu, W.-L. Dai, K. Fan, *Green Chem*. **2011**, *13*, 702–708.

[17] a) I. Tamiolakis, I. N. Lykakis, A. P. Katsoulidis, M. Stratakis, G. S. Armatas, *Chem. Mater*. **2011**, *23*, 4204–4211; b) I. Tamiolakis, I. N. Lykakis, A. P. Katsoulidis, C. D. Malliakas, G. S. Armatas, *J. Mater. Chem*. **2012**, *22*, 6919–6927.

[18] B. Li, W. Ma, J. Liu, C. Han, S. Zuo, X. Li, *Catal. Commun*. **2011**, *13*, 101–105.

[19] J. Alcañiz-Monge, G. Trautwein, M. C. Román-Martínez, *Solid State Sci*. **2011**, *13*, 30–37.

[20] J. Alcañiz-Monge, G. Trautwein, M. Pérez-Cadenas, M. C. Román-Martínez, *Microporous Mesoporous Mater*. **2009**, *126*, 291–301.

[21] Elemental analyses for some representative samples obtained upon treatment of the $(NH_4)_3[PMo_{12}O_{40}]$ precursor (**POM**) with $NH_4(CH_3CO_2)$. Calcd (%) for $(NH_4)_3[PMo_{12}O_{40}]$: H 0.64, Mo 61.36, N 2.24, P 1.65; found for **POM**: H 0.65, Mo 61.35, N 2.25, P 1.65; found for **POM-40**: H 0.63, Mo 61.40, N 2.28, P 1.62; found for **POM-60**: H 0.62, Mo 61.27, N 2.21, P 1.66; found for **POM-79**: H 0.65, Mo 61.13, N 2.16, P 1.64.

[22] a) G. B. McGarvey, J. B. Moffat, *J. Mol. Catal*. **1991**, *69*, 137–155; b) M. A. Schwegler, J. A. Peters, H. van Bekkum, *J. Mol. Catal*. **1990**, *63*, 343–351.

[23] M. Thommes, K. Kaneko, A. V. Neimark, J. P. Olivier, F. Rodriguez-Reinoso, J. Rouquerol, K. S. W. Sing, *Pure Appl. Chem*. **2015**, *87*, 1051–1069.

[24] J. H. De Boer, B. G. Linsen, Th. van der Plas, G. P. Zondervan, *J. Catal*. **1965**, *4*, 649–653.

[25] *Adsorption by Powders and Porous Solids. Principles, Methodology and Applications*, 2nd Edition (Eds.: J. Rouquerol, F. Rouquerol, P. Llewellyn, G. Maurin, K. S. W. Sing), Elsevier, Amsterdam, The Netherlands, **2014**.

[26] E. P. Barrett, L. G. Joyner, P. P. Halenda, *J. Am. Chem. Soc*. **1951**, *73*, 373–380.

[27] D. Cazorla-Amorós, J. Alcañiz-Monge, A. Linares-Solano, *Langmuir* **1996**, *12*, 2820–2828.

[28] K. Okamoto, S. Uchida, T. Ito, N. Mizuno, *J. Am. Chem. Soc*. **2007**, *129*, 7378–7384.

[29] a) S. J. Gregg, R. Stock, *Trans*. *Faraday Soc*. **1957**, *53*, 1355–1362; b) S. J. Gregg, M. M. Tayyab, *J. Chem. Soc., Faraday Trans. 1* **1978**, *74*, 348–358.

[30] S. Brunauer, P. H. Emmett, E. Teller, *J. Am. Chem. Soc*. **1938**, *60*, 309–319.

[31] M. M. Dubinin, in *Chemistry and Physics of Carbon, Volume 2* (Ed.: P. L. Walker, Jr.), Dekker, New York, USA, **1966**.

10.1002/chem.201604879

WILEY-VCH

Entry for the Table of Contents

FULL PAPER

Treating nanostructured microporous heteropolysalts with a basic agent allows for developing tailored mesoporosity in the solid material with control over both the mesoporous volume and the pore size. The development of mesoporosity originates from a process of alkaline degradation in the core of the nanocrystals that aggregate into the particles, and the resulting micro- and mesoporosity structures are independent.

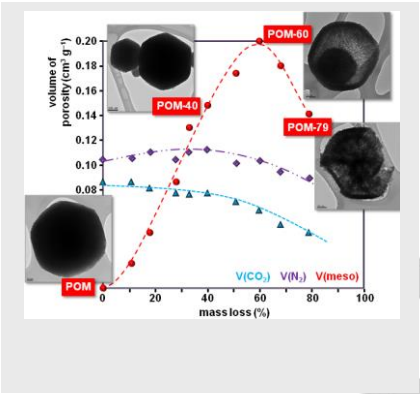

Juan Alcañiz-Monge, Guido Trautwein, Bouchra El Bakkali, Santiago Reinoso*

Page No. – Page No.

A Simple Approach to Develop Tailored Mesoporosity in Nanostructured Heteropolysalts